Robust PID control of propofol anaesthesia: uncertainty limits performance, not PID structure

Cava, José Manuel Gonzáles; Bagge Carlson, Fredrik; Troeng, Olof; Cervin, Anton; van Heusden, Klaske; Dumont, Guy A.; Soltesz, Kristian

Robust PID control of propofol anaesthesia: uncertainty limits performance, not PID structure

Jose M. Gonzalez-Cava[a], Fredrik Bagge Carlson[b], Olof Troeng[c], Anton Cervin[c], Klaske van Heusden[d], Guy A. Dumont[d], Kristian Soltesz[c]

[a]*Departamento de Ingeniería Informática y de Sistemas, Universidad de La Laguna, La Laguna 38200, Tenerife, Spain*
[b]*Acoustic Research Laboratory, National University of Singapore, Singapore*
[c]*Department of Automatic Control, Lund University, Lund 221 00, Sweden*
[d]*Department of Electrical and Computer Engineering, University of British Columbia, Vancouver, BC V6H 3V4, Canada*

Abstract

Background and Objective: New proposals to improve the regulation of hypnosis in anaesthesia based on the development of advanced control structures emerge continuously. However, a fair study to analyse the real benefits of these structures compared to simpler clinically validated PID-based solutions has not been presented so far. The main objective of this work is to analyse the performance limitations associated with using a filtered PID controller, as compared to a high-order controller, represented through a Youla parameter.

Methods: The comparison consists of a two-steps methodology. First, two robust optimal filtered PID controllers, considering the effect of the inter-patient variability, are synthesised. A set of 47 validated paediatric pharmacological models, identified from clinical data, is used to this end. This model set provides representative inter-patient variability Second, individualised filtered PID and Youla controllers are synthesised for each model in the set. For fairness of comparison, the same performance objective is optimised for all designs, and the same robustness constraints are considered. Controller synthesis is performed utilising convex optimisation and gradient-based methods relying on algebraic differentiation. The worst-case performance over the patient model set is used for the comparison.

Results: Two robust filtered PID controllers for the entire model set,

---

as well as individual-specific PID and Youla controllers, were optimised. All considered designs resulted in similar frequency response characteristics. The performance improvement associated with the Youla controllers was not significant compared to the individually tuned filtered PID controllers. The difference in performance between controllers synthesized for the model set and for individual models was significantly larger than the performance difference between the individual-specific PID and Youla controllers. The different controllers were evaluated in simulation. Although all of them showed clinically acceptable results, the robust solutions provided slower responses.

Conclusion: Taking the same clinical and technical considerations into account for the optimisation of the different controllers, the design of individual-specific solutions resulted in only marginal differences in performance when comparing an optimal Youla parameter and its optimal filtered PID counterpart. The inter-patient variability is much more detrimental to performance than the limitations imposed by the simple structure of the filtered PID controller.

1. Introduction

Adequate dosing of anaesthetic drugs is required to avoid awareness, maintain homeostasis, and reduce postoperative discomfort and recovery times in the post-anaesthesia care unit [1]. This requires continuous monitoring of the patient's anaesthetic state, enabling the anaesthesiologist to adapt drug titration as needed. It is this continuous decision-making process that has inspired extensive research on closed-loop control systems for anaesthetic drug dosing.

This work focuses on control of the hypnosis component of general anaesthesia, known as the Depth of hypnosis (DoH). We consider a closed-loop structure where the controller manages the infusion rate of the intravenous anaesthetic drug propofol to maintain a user-defined DoH setpoint, with the output of a cortical EEG monitor as measurement signal. The controller needs to attenuate the effect of the surgical disturbances. Failure to do so can result in patient awareness.The closed-loop system also needs to be insensitive to high frequency measurement noise typically associated with DoH monitors. Furthermore, and of high relevance to the design, the controller

must be robust against patient model uncertainty.

Properly tuned PID controllers have demonstrated adequate robustness, performance and safety in the clinical setting [2]. The simple structure and low parameter count are attractive features of the filtered PID controller, facilitating synthesis, implementation and verification. Different design approaches have been proposed to tune the proportional-integral-derivative parameters of the PID controllers [3]. More complex controllers have also been developed and clinically evaluated [4, 5]. Due to the absence of objective comparisons between controller structures, it remains unclear whether such advanced controller types in closed-loop anaesthesia could result in an increase in performance with maintained safety.

The design objectives commonly vary between published designs [6], and they are not always explicitly stated in works presenting manually tuned controllers. Variations in the patient cohort, type of surgery, drugs delivered, and the practical implementation of the controller may bias the comparison [7]. Furthermore, the sets of patient models used for controller synthesis vary across research groups, as does the dynamics on which the obtained controllers are evaluated. While published studies typically investigate the performance of a particular controller, they provide little insight into whether this performance is foremost limited by the type of controller or by some other factors such as the variability in the patient model set used for the synthesis.

The aim of this study is to directly compare the achievable performance of PID controllers and higher-order LTI structures for the regulation of the depth of hypnosis in anaesthesia. For this purpose, the same clinical and technical considerations need to be used for the synthesis of both structures. We have therefore formulated a robust performance synthesis problem with a clinically relevant control objective, which can be solved within both the filtered PID and Youla parameter frameworks. This enables comparison of achievable performance of a filtered PID controller, with that of an LTI controller of arbitrary order, for the same (uncertain) model set.

A Youla parameter, constituting an upper bound on performance for an LTI controller of arbitrary order, is synthesized. While methods for optimising filtered PID controllers over sets of plant models are considered herein, there exists no general [8], or in the considered context applicable, method to design optimal LTI controllers for a set of process dynamics. Therefore, a two-step comparison was proposed. First, the effect of the inter-patient variability on the closed-loop performance was studied. The performance achieved by a robust optimal PID synthesized for a set of patients was com-

pared with that achieved by individualized optimal PID controllers. Second, the performance of individualised PID controllers was compared with that of individual Youla parameters for the models in the considered set.

The contribution of this paper is twofold. In addition to the proposed method that enables systematic comparison between a filtered PID controller and an optimal LTI controller for DoH control, our illustrative example shows that the room for improvement when increasing controller order beyond that of a filtered PID is marginal when a model set featuring representative inter-patient variability is considered.

2. Modelling the anaesthetic process

2.1. Patient models

Pharmacokinetic-pharmacodynamic (PKPD) models are used in anaesthesia to describe the relationship between the hypnotic drug (propofol) infusion rate, and its effect on a clinical variable (the DoH) [9].

The comparison presented in this work was made using a set $\mathcal{P}$ of 47 paediatrics PKPD models [10]. The models were identified from clinical data and then linearised as described in [11]. The main motivation for using this set of linearised models is that robust PID controllers, similar to the ones considered herein, have been designed for it, and extensively validated both in simulation and clinically [12].

Variability can be directly characterised by the linearised models of the set $\mathcal{P}$. A more conservative characterisation is provided by the unstructured additive uncertainty model

$$P_\Delta(i\omega) = \{P_0(i\omega) + \rho(\omega)\Delta : \Delta \in \mathbb{C}, \|\Delta\|_\infty < 1\}, \qquad (1)$$

where P_0 is a nominal model, Δ is any point within the unit disc in the complex plane, and ρ is the uncertainty radius. The response $P_\Delta(i\omega)$ was chosen to frequency-wise minimise $\rho(\omega)$, while covering $\mathcal{P}(i\omega)$. This results in a convex program, enabling efficient computation of P_0 and ρ from $\mathcal{P}$, as described in [13]. Both $\mathcal{P}$ and P_Δ were considered as descriptions of inter-patient variability in our study.

Note that these models and uncertainty description focus on uncertainty resulting from inter-patient variability, being the most challenging uncertainty source from a control synthesis perspective, and relatedly, the one that has received most research attention. Uncertainty can also arise as a

4

consequence of intra-patient variability (e.g. haemodynamics affecting drug distribution and metabolism) and also as a consequence of limited parameter identifiability from underlying modelling experiments [14, 15].

2.2. Equipment models

The Bispectral Index (BIS) monitor has been used to measure the DoH in a majority closed-loop controlled propofol anaesthesia systems [16]. We instead assume the use of the NeuroSense WAV$_{CNS}$ monitor. It is similar to the BIS, but comes with the advantage of time-invariant response dynamics [17]

$$M(s) = \frac{1}{(8s + 1)^2},$$

(2)

making it more suitable for closed-loop control applications [18].

The monitor dynamics (2) were incorporated in our study through series connection with the patient model.

Dynamics of modern remote-controlled infusion pumps are essentially static and linear, with negligible quantisation effects. In addition, bandwidth and titration precision of these pumps are high, relative to the requirements imposed on a closed-loop propofol anaesthesia system. Consequently, no explicit actuator model has been employed.

2.3. Disturbance models

Two main exogenous disturbances were considered in this study. First, surgical stimuli act as disturbances, increasing the DoH, unless counteracted. As suggested in [19], they were modelled as steps added to the patient output. Second, measurement noise was added to the DoH monitor output. A white noise model, previously identified from data [19], was used.

3. Optimisation-based controller design

3.1. Performance and robustness

Closed-loop DoH control involves two problems: a servo problem, associated with the induction of anaesthesia, during which the patient state is transitioned from aware to a setpoint DoH; a regulator problem, associated with maintenance of anaesthesia, aimed at disturbance attenuation in the vicinity of the setpoint. It is good control engineering practice to separate the two using a two-degree-of-freedom (2DOF) design, as suggested in [20],

where the regulator problem is first solved by a feedback controller, that is then augmented with a feedforward controller addressing setpoint tracking. This work considers the regulator problem.

A block diagram illustrating the closed-loop system is shown in Figure 1. The control objective is to attenuate the disturbance, d, from the DoH, z. Considering that sudden large deviations from the setpoint are clinically worse than more persistent small setpoint deviations, the $\mathcal{L}_2$ norm of the monitored DoH, y, resulting from a disturbance step, d, was minimized.
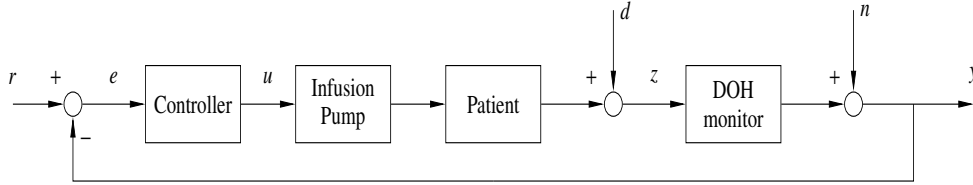

Figure 1: Block diagram of the closed-loop system. The signals are: DoH setpoint, r; propofol infusion rate, u; DoH, z; measured DoH, y; surgical disturbance, d; measurement noise, n.

To ensure robustness of the design, $\mathcal{H}_\infty$ constraints on the sensitivity function S, and its complement, $T = 1 - S$, were imposed. Constraining $\|T\|_\infty$ and $\|S\|_\infty$ provides robustness to additive process perturbations and loop-transfer perturbations [21]. Measurement noise was attenuated by imposing an $\mathcal{H}_2$ constraint on the transfer function KS from noise, n, to control signal, u. The noise sensitivity constraint was expressed using the $\mathcal{H}_2$, since the outcome of limiting the $\mathcal{H}_\infty$ norm depends heavily on for which frequency, with respect to the closed-loop bandwidth, it is attained [22]. The constraint levels (M_s, M_t and M_{ks}) were chosen to match worst case values of the constrained functions, evaluated over the considered inter-patient variability model, with a previously clinically evaluated PID controller in the loop [12]. These constraints limit maximal magnitudes of sensitivity and complementary sensitivity, and bound admissible energy transfer from measurement noise to control signal. They do not limit performance more than required for adequate robustness. In particular, it is easy to devise examples with other plant dynamics, where a Youla design would outperform a PID counterpart under the given constraints.

Response undershoot was limited to 10 WAV$_{\text{CNS}}$, preventing the worst-case undershoot associated with the 50 WAV$_{\text{CNS}}$ to bring the DoH outside the recommended 40–60 WAV$_{\text{CNS}}$ interval for general anaesthesia. With

6

modern infusion pumps, prevention of actuator wear is not a motivation for limiting control signal noise. However, slew rate limitations and the risk of the supervising anaesthesiologist putting a controller with violently varying output into manual mode would be [23].

Filtered PID controllers, robust over the model set, $\mathcal{P}$, and the uncertain model, P_Δ, were synthesised, alongside individual filtered PID controllers for each each of the 47 models in $\mathcal{P}$. The latter were compared with Youla parameters, individually optimised for the same 47 models. First, this comparison quantified the benefit of increasing controller order. Second, the comparison between the individualised PID controllers with those optimized to be robust over $\mathcal{P}$ and P_Δ, respectively, quantified the performance limitations imposed by inter-patient variability. Main considerations for the optimisation of the different controllers are presented in the next subsections.

3.2. PID controllers

A general description for the synthesis of the PID controllers included in the comparison is presented in this section. Robust filtered PID controllers in the form

$$K(s) = C(s)F(s) \tag{3}$$

$$C(s) = k_p + k_i \frac{1}{s} + k_d s \tag{4}$$

$$F(s) = \frac{1}{T^2 s^2 + 2\zeta T s + 1} \tag{5}$$

were synthesised. Parameters $[k_p,\ k_i,\ k_d]$ of the PID controller (4) were co-optimised with parameters $[T,\ \zeta]$ of the filter (5).

The parametrisation of K resulted in a non-convex synthesis problem that was approached with a two-stage method. First, a global optimisation, based on simulated annealing (SA), was performed [24], with logarithmic barrier functions representing the constraints. Since SA is a gradient-free method, it provides no means to verify local optimality. Consequently, the second stage comprised gradient-based optimisation by means of the method of moving asymptotes (MMA) [25]. The optimisation methods were implemented using the Julia language package ControlSystems.jl [26] in combination with forward-mode automatic differentiation [27]. Key implementation aspects are reviewed in [28].

7

The optimisation was performed over a uniform frequency grid

$$\Omega = \{\omega_1, \ldots, \omega_N\}, \qquad \omega_k = \frac{k\pi}{NT_s},$$

where the number of frequency points, $N = 2^{11}$, was numerically verified to lie sufficiently dense for the problem at hand. The sampling period was set to $T_s = 5\,\text{s}$, matching the actuation interval in the control system for which the models are intended [12].

3.2.1. PID control based on the model set

The filtered PID controller was optimised by maximizing the worst-case performance over the patient model set $\mathcal{P}$ while satisfying robustness and undershoot constraints for each patient model in $\mathcal{P}$:

$$\min_{K} \quad \max_{\forall k \in \{1, \ldots, \#(\mathcal{P})\}} \left\| S_k \frac{1}{i\omega} \right\|_2^2 \tag{6}$$

$$\begin{array}{ll} \text{subject to} & \|S_k\|_\infty \leq M_s \\ \scriptstyle \forall k \in \{1, \ldots, \#(\mathcal{P})\} & \\ & \|T_k\|_\infty \leq M_t \\ & \|KS_k\|_2 \leq M_{ks} \\ & \mathcal{F}^{-1}\left(S_k \frac{1}{i\omega} \right) \geq m_y. \end{array}$$

3.2.2. PID based on the uncertain model

Inter-patient variability was represented by $P_\Delta(i\omega)$, describing the set of all possible responses at frequency ω. The problem of optimisation of the worst-case performance while satisfying worst-case constraints over $P_\Delta(i\omega)$

8

is given by

$$\min_{K} \quad \frac{1}{\pi} \int_0^\infty \overline{S}^2 \frac{1}{\omega^2} d\omega \tag{7}$$

$$\text{subject to} \quad |P_0 KM + 1| - \rho |KM| - \frac{1}{M_s} \geq 0$$
$$\forall \omega$$

$$|P_0 KM + f(M_t)| - \rho |KM| - \frac{f(M_t)}{M_t} \geq 0$$

$$\|\overline{KS}\|_2 \leq M_{KS}$$

$$\min_{P_\Delta} \left(\mathcal{F}^{-1} \left(S_\Delta \frac{1}{i\omega} \right) \right) \geq m_y,$$

where

$$f(M_t) = \frac{M_t^2}{M_t^2 - 1}$$

and

$$\overline{S} = \frac{1}{|P_0 KM + 1| - \rho |KM|} \tag{8}$$

represents the worst-case sensitivity in terms of the optimisation objective generated by P_Δ. A detailed explanation of the derivations for the worst-case expressions in (7) and (8) is provided in the Appendix.

The last inequality of (7), where S_Δ represents any frequency-wise reali-sation of $(1 + PK)^{-1}$ with $P \in P_\Delta$, limits load-response undershoot to m_y. Minimisation under P_Δ generates the worst case for the constraint under S_Δ. Undershoot was limited by enforcing that $y_k \geq m_y$ is fulfilled for each corresponding time-domain sample

$$y_k = \frac{1}{N} \sum_{n=0}^{N-1} Y_n e^{\frac{2\pi n}{N} i} \tag{9}$$

of the response y. Each Y_n needs to be selected from a disc in the complex plane, generated by P_Δ, before the inverse Fourier transform (9) is applied. The radii of these discs are given by the expression (A.6), provided in the Appendix. The smallest contribution to y_k from disc y_N is ρ_n, resulting in the bound

$$y_k \geq y_{k,0} - \sum_{n=0}^{N-1} \rho_n. \tag{10}$$

3.2.3. PID control based on the individual models

A similar formulation to (6) was considered for the optimisation of the individualised filtered PID, in which maximisation over $k \in \{1, \ldots, \#(\mathcal{P})\}$ was replaced by optimising individual controllers for each patient model k.

3.3. Youla synthesis

The Youla parametrisation characterises all stabilising controllers, K, for a linear plant, P. Using a suitable representation of a general controller transfer function, it is possible to apply convex optimisation to search for the optimal controller. For a stable plant, the Youla parametrisation becomes particularly simple. Introducing the Youla parameter

$$Q = \frac{K}{1 + PK}, \tag{11}$$

the sensitivity function and its complement can be expressed as

$$T = PQ \tag{12}$$
$$S = 1 - PQ \tag{13}$$

while the control signal response to measurement noise is given by $KS = Q$.

Transient responses were evaluated over $T = 8000\,\mathrm{s}$, being a sufficient horizon considering propofol PK dynamics. The Youla parameter Q was expressed using the Ritz approximation

$$Q_d(z) = Q_0(z) + \sum_{k=1}^{N_q} x_k Q_k(z) \tag{14}$$

where x_k are the scalar variables to be optimised, and $Q_k(z) = z^{k-1}$ represents a discrete-time shift. The constant term of (14) is given by

$$Q_0(z) = \frac{K_{\mathrm{ind},d}(z)}{1 + P_d(z)K_{\mathrm{ind},d}(z)}, \tag{15}$$

where

$$K_{\mathrm{ind},d}(z) = \mathcal{FOH}(K_{\mathrm{ind}}(s), h) \tag{16}$$

$$P_d(z) = \mathcal{FOH}(P(s), h) \tag{17}$$

10

are the first-order-hold discretisations of the optimal individualised filtered PID controller and the plant, respectively.

The same frequency grid and sampling period were used for the Youla and filtered PID designs. The corresponding cost to be minimised was

$$J = \sum_{k=0}^{T/h} y^2(k). \tag{18}$$

The aforementioned robustness constraints on S, T and KS, as well as the undershoot constraint on y were introduced.

To guarantee that J converges as $t \to \infty$, the controller must have integral action. This was enforced by adding the steady-state constraint

$$\left| Q_d(1) - \frac{1}{P_d(1)} \right| < \epsilon \tag{19}$$

for some small ϵ (10^{-7} was used here). All considered constraints are closed-loop convex, meaning that a solution can be found efficiently. Once the optimal Q_d is found, the controller is recovered as

$$K_d = \frac{Q_d}{1 - Q_d P_d}. \tag{20}$$

The optimisation problem was specified and solved in MATLAB using the CVX optimisation library with the MOSEK solver. All solutions were checked for constraint violations between grid points.

4. Results

4.1. Analysis of the optimisation

Table 1 provides an overview of the resulting controllers. The parameter values obtained through the optimisation are shown in Table 2 for the robust filtered PID designs. The choice of $N_q = 400$ parameters of the Youla controller, Q_K, was deemed sufficient , and further increase resulted in negligible performance gain. Since the high parameter count of Q_K renders tabulation infeasible, Bode plots for the analysis of the frequency response of each controller are presented instead. Figure 2 reveals a high degree of similarity between the considered designs. The main difference between the individually optimised PID controllers, K_{ind}, and their Youla parameter counterparts,
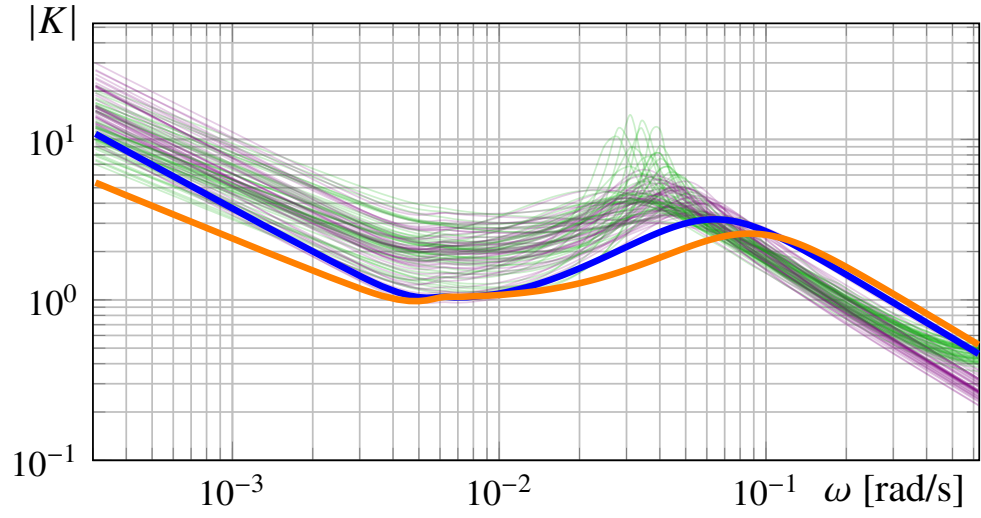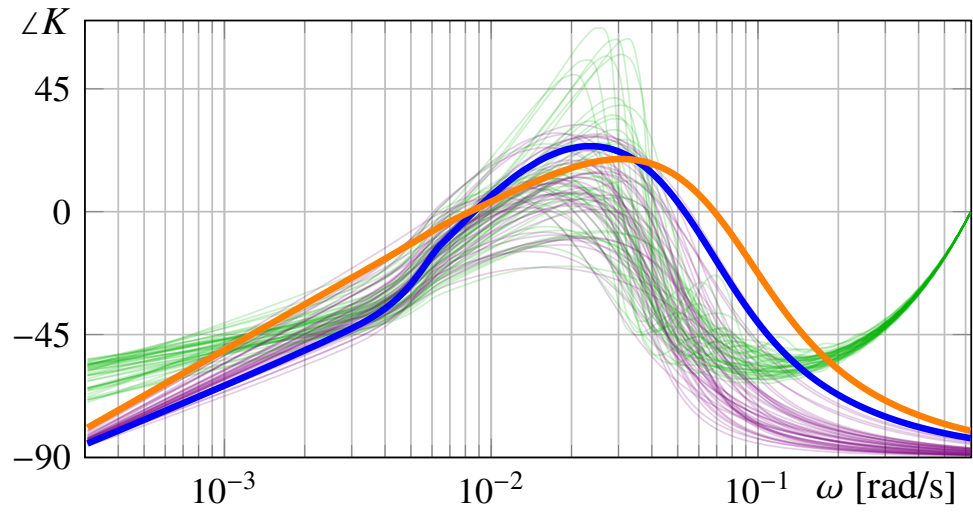
Figure 2: Controller Bode plots. a) shows magnitudes, $|K(i\omega)|$; b) shows phases, $\angle K(i\omega)$. Colours according to Table 1.

Table 1: List of evaluated Youla parameters and filtered PID controllers, and the colour used to represent them in figures of Section 4.

Controller	Colour	Description
K_{set}	blue	PID for patient set
K_Δ	orange	PID for additive uncertainty model
K_Q	green	individualised Youla controller
K_{ind}	violet	individualised PID controller

Table 2: Parameters of the considered filtered PID controllers. Parameters correspond to the ideal serial PID form $K_p(1 + (T_i s)^{-1} + T_d s)$. The filter parameters are presented as in (5). Units are: K_p [mg/kg/min WAV$_{\text{CNS}}$]; T_i [s]; T_d [s]; T_f [s]. The relative damping ζ is dimensionless.

	K_p	T_i	T_d	T_f	ζ
K_{set}	1.04	314	65.1	15.3	0.71
K_Δ	1.05	644	38.7	11.1	0.73

K_Q, lies in the mid-frequency range, where the additional degrees of freedom of K_Q provided a phase advance in the range of 0.01–0.05 rad/s. The main difference between the filtered PID designs were for low frequencies.

Figure 3 shows the distribution of the optimisation cost when applying the considered controllers over the patient model set $\mathcal{P}$. Cost values were normalised by the maximum cost $\alpha = 316$, attained over $\mathcal{P}$ with the clinically verified filtered PID controller, K_C. For a particular model, it was observed that the above-mentioned relative phase advance of the Youla design in the mid-frequency range resulted in limited performance improvement over the individually tuned filtered PID controllers. However, including uncertainty from the inter-patient variability resulted in a significantly worse performance as seen by comparing either of K_{set} or K_Δ with K_{ind}.

Resulting sensitivity and complementary sensitivity magnitudes are shown in Figure 4. The constraint levels, $M_s = 2.55$ and $M_t = 2.08$, correspond to the worst case $\mathcal{H}_\infty$ norms obtained when evaluating K_C over $\mathcal{P}$. The $\mathcal{H}_2$
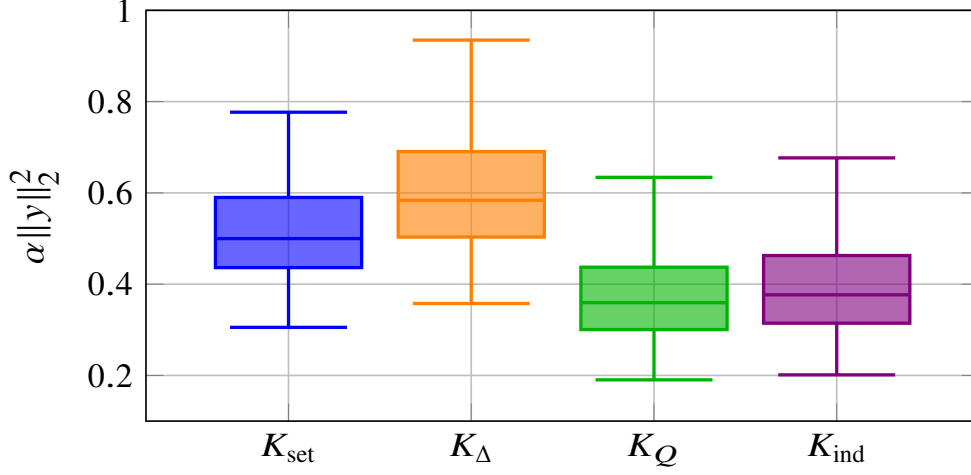
Figure 3: Distribution of optimisation cost $\|y\|_2^2$ over the patient model. Colours according to Table 1.

norms and the Bode magnitudes of the underlying KS were computed for the analysis of the noise sensitivity constraint. Results are shown in Figures 5 and 6, respectively. The noise sensitivity constraint was active for each controller type except K_Δ. Specifically, it was active for each of the 47 models in $\mathcal{P}$ under K_{ind} and K_Q. In addition, at least one patient model of the set reached the constraint when optimising K_{set}. As a result, it could be noted that the performance was limited by the constraint level on noise sensitivity, KS, in three of the four proposed designs.

The results of the closed-loop patient output to a step disturbance when considering the linearised patient models is shown in Figure 7. The undershoot constraint was only active for K_Δ. However, as a consequence of Δ being a conservative uncertainty description, K_Δ resulted in fulfilment of the undershoot constraint when evaluating the controller over the 47 individual patient models of $\mathcal{P}$.

4.2. Simulations

Controller performance of the obtained controllers were evaluated in a simulation using the 47 *nonlinear* patient models, from which the linear models comprising $\mathcal{P}$ were obtained. A DoH setpoint of 50 WAV$_{\text{CNS}}$ was considered. With the systems in stationarity at this setpoint, a step disturbance of magnitude 10 WAV$_{\text{CNS}}$ was applied at $t = 0$. The outcome is shown in
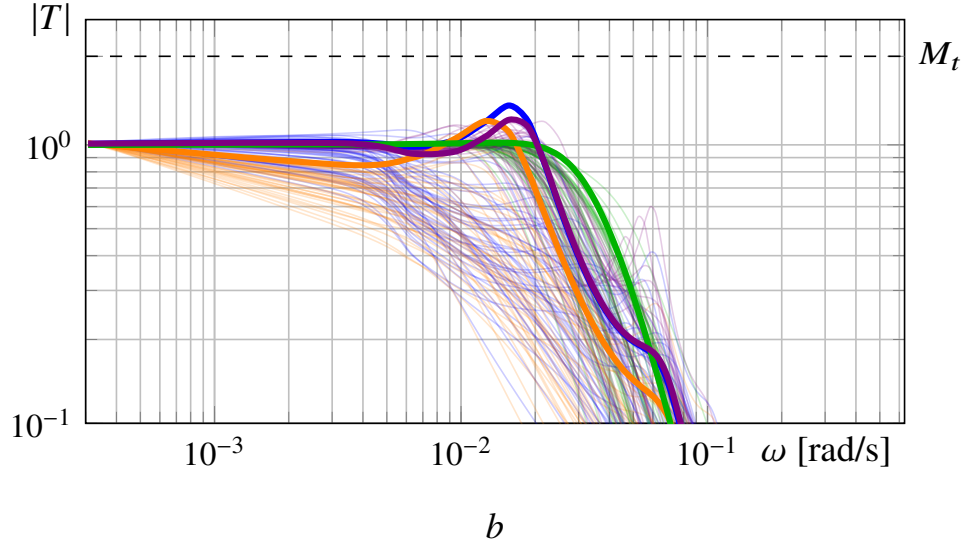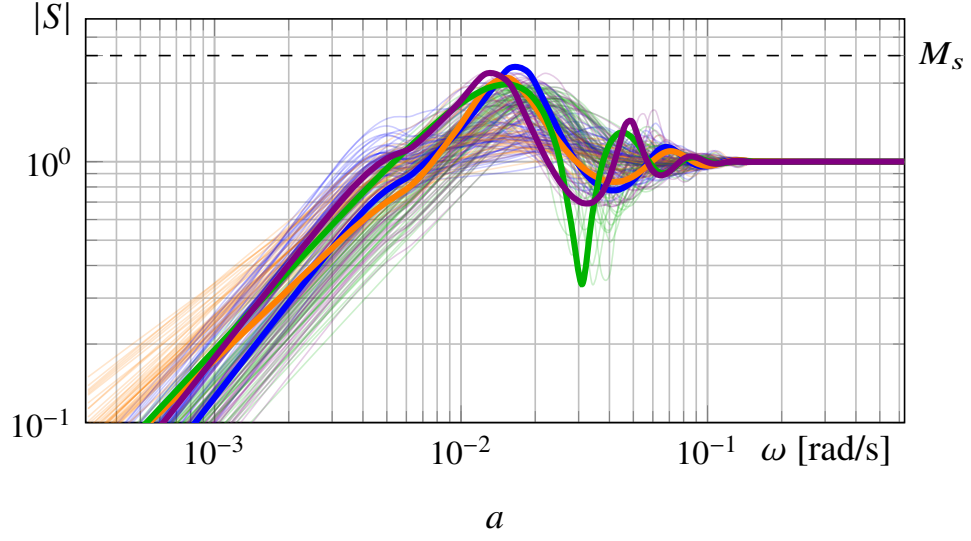
Figure 4: Magnitudes of a) sensitivity $|S(i\omega)|$ and b) complementary sensitivity $|T(i\omega)|$ for the considered designs. The horizontal dashed black line shows the constraint levels. Thick lines show the worst-case constraint level for each considered controller type. Colours according to Table 1.
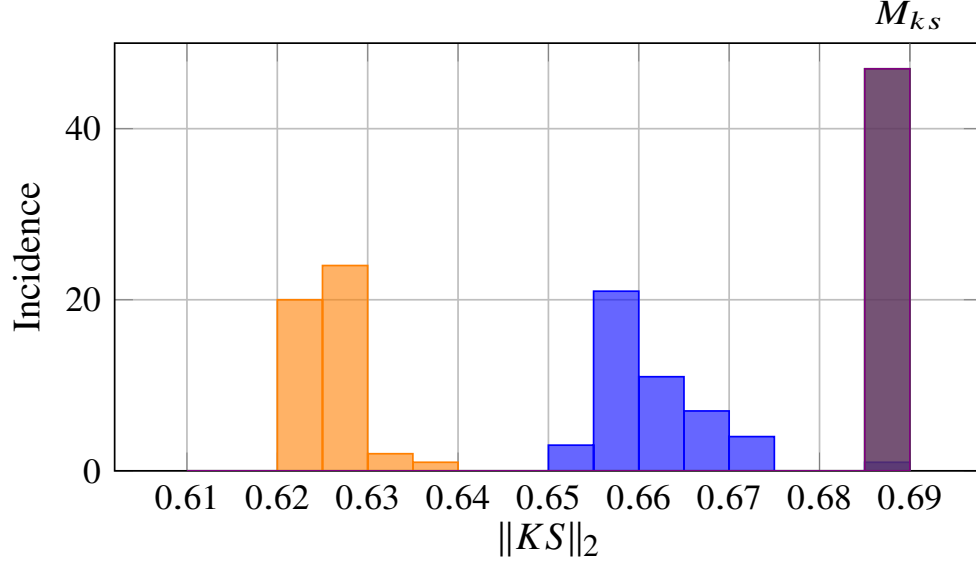
Figure 5: Distribution of noise sensitivity $\mathcal{H}_2$ norm, $\|KS\|_2$, of the considered controllers over the patient model set. The vertical dashed black line shows the constraint level, M_{ks}. Colours according to Table 1.
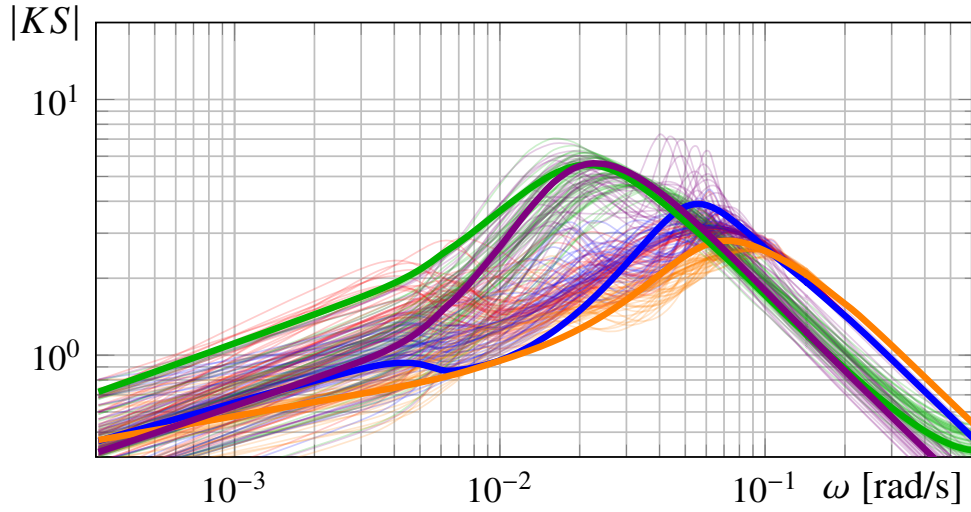

Figure 6: Noise sensitivity magnitude $|K(i\omega)S(i\omega)|$ for the considered design. Thick lines correspond to the closed-loop generating the worst $\|KS\|_2$ for each controller type. Colours according to Table 1.
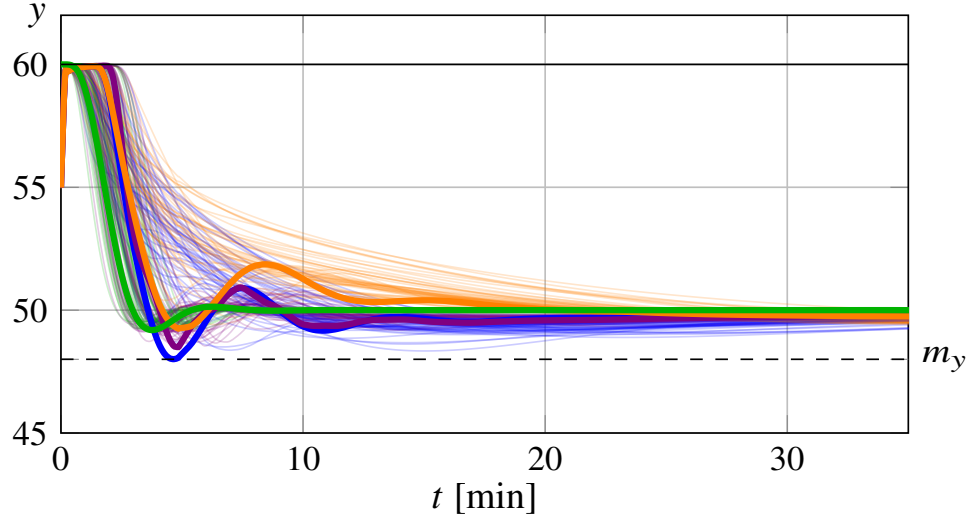
16

Figure 7: Closed-loop response $y(t)$ resulting from applying an additive output disturbance of magnitude 10 WAV$_\mathrm{CNS}$ (solid black line) to each model in the set. Thick lines show the responses of maximal undershoot for each considered controller type. The dashed black line shows the undershoot constraint level m_y. Colours according to Table 1.

Figure 8. All designs provided admissible disturbance responses, similar to those resulting from the linearised models. These results show that the controllers maintain the DoH within the recommended 40–60 WAV$_\mathrm{CNS}$ range during the maintenance phase, in face of disturbances and the design model mismatch caused by the nonlinearity.

5. Discussion

This simulation study has compared the achievable performance of a widely used and clinically validated PID-based structure for DoH control to that involving a more advanced linear time-invariant controller of arbitrary high order. All considered controllers were optimised using the same performance and robustness criteria. The effect of the inter-patient variability on the performance was analysed. Both synthesis and evaluation were based on a set of previously published and verified PKPD patient models. All the designs were performed for linearised versions of the patient models. Consequently, the resulting controllers were evaluated together with the underlying nonlinear models to validate the results. The comparison showed
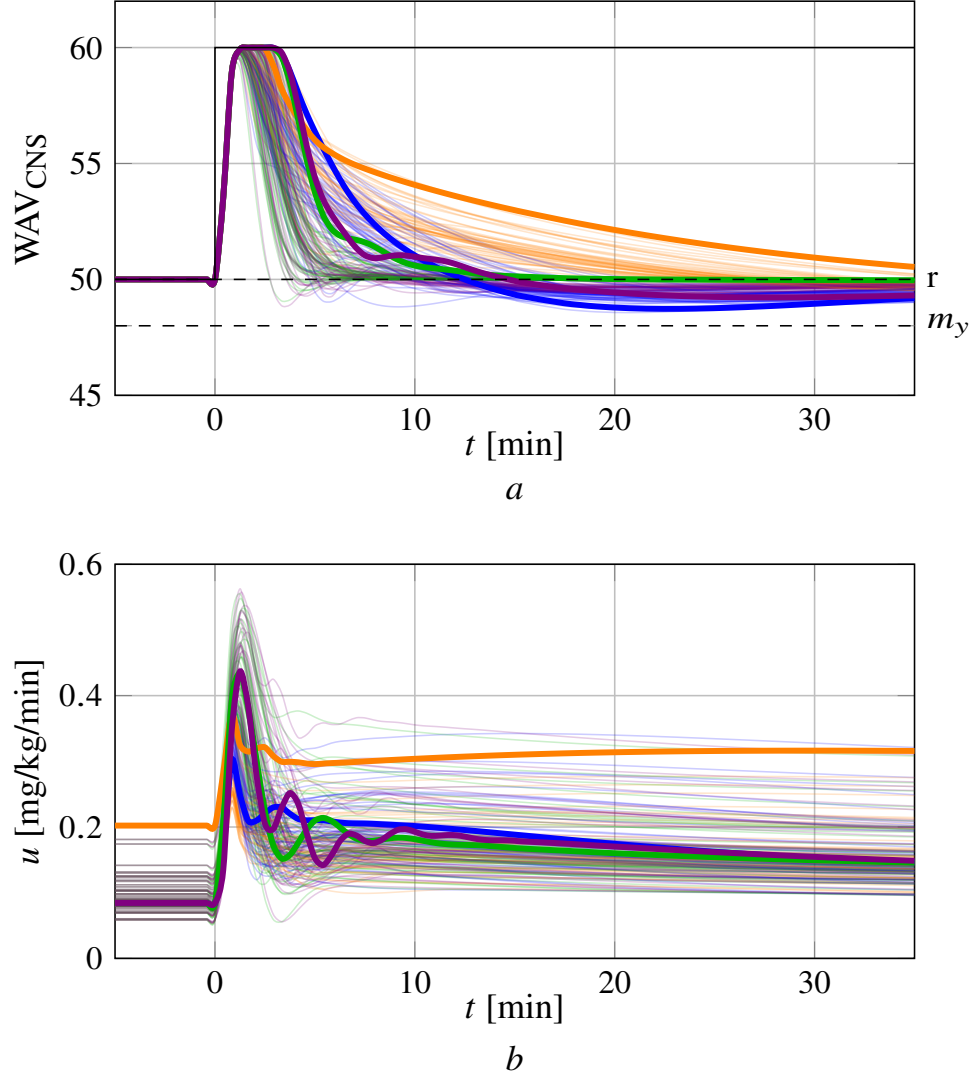
Figure 8: Closed-loop responses of the *nonlinear* patient models when applying a simulated surgical stimulation. a) shows simulated NeuroSense monitor responses. The disturbance is shown in solid black; the dashed black line represents the setpoint $r = 50$ WAV$_{\text{CNS}}$, and the undershoot constraint level m_y imposed. b) shows the corresponding infusion profiles u. Thick lines show the highest cost over the patient model set for each considered controller type. Colours according to Table 1.

that increasing controller order beyond that of a filtered PID, resulted in only marginal performance gains, and further improvements were prevented by the inter-patient variability. Taking additional uncertainty sources, such as intra-patient variability and model parameter uncertainty associated with identification from experimental data, into account, will further diminish the margin for improvement.

The objective used in the current comparison was to minimise the $\mathcal{L}_2$ norm of the measured DoH response resulting from the disturbance model. To introduce further robustness and associated conservatism, an uncertainty description from the model set was generated and considered for the synthesis of a robust controller as proposed in [13]. This approach enables the use of model-based designs, from a small number of models with significant spread in frequency response. Since a set of models was considered here, worst-case performance over the model set was optimised, while ensuring that each imposed constraint was fulfilled for each model of the set. While optimising mean or median performance constitutes possible alternatives, the worst case was chosen here since it introduces safety through conservatism.

Disturbance attenuation was balanced against undershoot, through imposing a constraint of 10 WAV$_{\mathrm{CNS}}$ on the latter. Relatedly, a trade-off between performance and control signal activity was introduced through constraining the noise sensitivity function. It could be noted that the associated constraint levels $M_s = 2.55$ and $M_t = 2.08$ exceeded the typical recommendation [21]. The reason is that robustness to inter-patient variability was enforced to a large degree by taking the model set into account, as opposed to designing for a single patient model and enforcing robustness across the set using the mentioned constraint levels. Here, M_s and M_t should instead be viewed as providing additional robustness, ensuring stability for patient models which were not fully represented by those in $\mathcal{P}$.

The presented methodology could be applied also to other clinically representative model sets or synthesis problem formulations. Studies conducted to date show that there is a large similarity between the pharmacological behaviours described by the PKPD models proposed for adults and children, see e.g. [29]. On a similar note, in some applications a slightly differing objective could be preferable. In [12], a PID controller for propofol anaesthesia was optimised and clinically evaluated. Limiting the time of induction for anaesthesia was more heavily emphasized, resulting in parameters values differing slightly from the ones reported here. In addition, a comparison between a PID controller and a higher-order model-based controller was con-

ducted in [30]. However, both controllers included in the comparison were manually tuned. Although the same design objective was considered for both controllers, different design criteria were implemented.

The main limitation of our study lies in the infeasibility of finding the optimal Youla parameter for a set of models. (While unknown, its performance would be upper bounded by K_Q and lower bounded by K_{set}.) This is why we have compared optimal Youla parameters for individual patient models to corresponding optimal filtered PID controller. The two rightmost boxes of Figure 3 reveal that there is very little difference in performance between these two designs. Separate comparison between the individualized filtered PID controllers (K_{ind}), and those designed to be perform robustly across the inter-patient variability (K_{set}, K_Δ) reveals that the main performance difference between designs included in the study can instead be attributed to the inter-patient variability.

6. Conclusion

Given clinically imposed requirements on robustness in combination with representative inter-patient variability, increasing controller order beyond that of a filtered PID controller does not significantly increase achievable performance in propofol DoH control. Relatedly, there is a significant discrepancy between the achievable performance when considering an individual patient model compared to a model capturing representative variability within a target population. To conclude, there is little to gain by increasing controller complexity, unless model uncertainty stemming from inter-patient variability is reduced.

7. Acknowledgement

Appendix A. Appendix

Expressions pertaining to the studied optimisation problem are derived below. The optimisation objective of (7) is to minimise the (squared) $\mathcal{L}_2$ norm of the output, resulting from a load step disturbance:

$$\min_K \max_{P_\Delta} \left\| S_\Delta \frac{1}{iw} \right\|_2^2 = \min_K \max_{P_\Delta} \frac{1}{\pi} \int_0^\infty \left| S_\Delta \frac{1}{iw} \right|^2 dw, \qquad (A.1)$$

where

$$S_\Delta = \frac{1}{1 + P_0 KM + |KM| \, \rho\Delta} \qquad (A.2)$$

is the uncertain sensitivity function generated by P_Δ. Introducing

$$\overline{S} = \max_{P_\Delta} |S_\Delta|,$$

the minimisation of (A.1) can be formulated as

$$\min_K \frac{1}{\pi} \int_0^\infty |S_\Delta|^2 \frac{1}{w^2} \, dw = \min_K \frac{1}{\pi} \int_0^\infty \overline{S}^2 \frac{1}{w^2} \, dw.$$

The expression (8) for $\overline{S}$ is obtained by taking the modulus of (A.2). Let φ be the argument of the term $1 + P_0 KM$ in the denominator of (A.2). Maximisation of (8) under $\rho\Delta$ then occurs for a point on the boundary of Δ with argument $-\varphi$. The modulus of S_Δ at this point is given by (8).

In the absence of uncertainty, $\mathcal{H}_\infty$ constraints on S and T are equivalent to the loop transfer function, L avoiding discs in the Nyquist plane for all considered frequencies:

$$|L - c| - r \geq 0. \qquad (A.3)$$

The centres c_* and radii r_* of these discs are

$$c_s = -1, \quad r_s = \frac{1}{M_s}, \quad c_t = -\frac{M_t^2}{M_t^2 - 1}, \quad r_t = \frac{M_t}{M_t^2 - 1},$$

where the subscripts s and t correspond to the sensitivity and complementary sensitivity constraints, respectively. See, [31] for further details. Generalisations to the case involving the additive uncertainty $\rho\Delta$, comprises maximising (A.3) under P_Δ. The methodology is the same as used to obtain the

expression (8) from (A.2), resulting in

$$|P_0KM + 1| - \rho|KM| - \frac{1}{M_s} \geq 0$$

$$\left| P_0KM + \frac{M_t^2}{M_t^2 - 1} \right| - \rho|KM| - \frac{M_t}{M_t^2 - 1} \geq 0.$$

The (squared) $\mathcal{H}_2$ constraint on noise sensitivity can be expressed as

$$\max_{r\Delta} \frac{1}{\pi} \int_0^\infty |K|^2 \ |S_\Delta|^2 \ dw \leq M_{ks}^2$$

$$\Leftrightarrow \quad \frac{1}{\pi} \int_0^\infty |K|^2 \ \overline{S}^2 \, dw \leq M_{ks}^2.$$

The undershoot constraint $y \geq m_y$ is enforced point-wise in the step response. This is achieved by constraining

$$\underline{y}_k = \min_{P_\Delta} \mathcal{F}^{-1} \left(S_\Delta \frac{1}{i\omega} \right), \tag{A.4}$$

where $\underline{y}_k$ is the minimum of the response y under P_Δ at sample k and $\mathcal{F}^{-1}$ the inverse Fourier operator. The minimum $\underline{y}_k$ of (A.4) can be expressed as

$$\underline{y}_k = y_{k,0} - \frac{1}{N} \sum_{n=0}^{N-1} \bar{\rho}_n, \tag{A.5}$$

where $y_{k,0}$ is the inverse Fourier transform of the response with the nominal model P_0 in the loop. For each frequency grid point, indexed by n in (A.5), the worst case contribution $\bar{\rho}_n$ can be obtained similarly to how $\bar{S}$ was obtained from S_Δ:

$$\bar{\rho}_n = \frac{|KM| \, \rho}{|1 + P_0KM|^2 - |KM|^2 \, \rho^2} \frac{1}{2\pi\omega_n}. \tag{A.6}$$

Like before, the angular frequency argument (here ω_n) has been dropped from (A.6), to facilitate readability.

References

[1] M. Ilyas, M. F. U. Butt, M. Bilal, K. Mahmood, A. Khaqan, R. Ali Riaz, A Review of Modern Control Strategies for Clinical Evaluation of Propofol Anesthesia Administration Employing Hypnosis Level Regulation, BioMed Research International 2017 (2017) 1–12.

[2] J. Reboso, J. Gonzalez-Cava, A. León, J. Mendez-Perez, Closed loop administration of propofol based on a Smith predictor: A randomized controlled trial, Minerva Anestesiologica 85 (2019) 585–593.

[3] L. Merigo, M. Beschi, F. Padula, N. Latronico, M. Paltenghi, A. Visioli, Event-Based control of depth of hypnosis in anesthesia, Computer Methods and Programs in Biomedicine 147 (2017) 63–83.

[4] I. Naşcu, A. Krieger, C. M. Ionescu, E. N. Pistikopoulos, Advanced model-based control studies for the induction and maintenance of intravenous anaesthesia, IEEE Transactions on Biomedical Engineering 62 (2015) 832–841.

[5] C. D. Côté, P. J. Kim, Artificial intelligence in anesthesiology: Moving into the future., University of Toronto Medical Journal 96 (2019).

[6] F. Padula, C. Ionescu, N. Latronico, M. Paltenghi, A. Visioli, G. Vivacqua, Optimized PID control of depth of hypnosis in anesthesia, Computer Methods and Programs in Biomedicine 144 (2017) 21–35.

[7] M. M. R. F. Struys, T. De Smet, S. Greenwald, A. R. Absalom, S. Bingé, E. P. Mortier, Performance Evaluation of Two Published Closed-loop Control Systems Using Bispectral Index Monitoring, Anesthesiology 100 (2004) 640–647.

[8] V. Blondel, Simultaneous stabilization of linear systems, Macmillan, 1994.

[9] A. M. Araújo, H. Machado, P. G. Pinho, P. Soares-da-Silva, A. Falcão, Population Pharmacokinetic-Pharmacodynamic Modeling for Propofol Anesthesia Guided by the Bispectral Index (BIS), The Journal of Clinical Pharmacology (2019).

23

[10] K. van Heusden, M. Ansermino, K. Soltesz, S. Khosravi, N. West, G. Dumont, Quantification of the variability in response to propofol administration in children, IEEE Transactions on Biomedical Engineering 60 (2013) 2521–2529.

[11] K. Van Heusden, J. M. Ansermino, G. A. Dumont, Robust MISO control of propofol-remifentanil anesthesia guided by the neurosense Monitor, IEEE Transactions on Control Systems Technology 26 (2018) 1758–1770.

[12] K. van Heusden, K. Soltesz, E. Cooke, S. Brodie, N. West, M. Görges, J. M. Ansermino, G. A. Dumont, Optimizing robust PID control of propofol anesthesia for children; design and clinical evaluation, IEEE Transactions on Biomedical Engineering 66 (2019) 2918–2923.

[13] K. Soltesz, K. van Heusden, M. Hast, M. Ansermino, G. Dumont, A synthesis method for automatic handling of inter-patient variability in closed-loop anesthesia, in: American Control Conference, Boston, Massachusetts, USA, pp. 4877–4882.

[14] M. Le Guen, L. Ngai, T. Chazot, M. Fischler, Closed-loop anesthesia: a systematic review, Minerva anestesiologica 82 (2015) 573–581.

[15] K. Soltesz, K. van Heusden, G. Dumont, Models for control of intravenous anesthesia, in: D. Copot (Ed.), Automated drug delivery in anesthesia, Elsevier, Amsterdam, Netherlands, 2019, pp. 119–156.

[16] M. H. Kuizenga, H. E. Vereecke, M. M. Struys, Model-based drug administration, Current Opinion in Anaesthesiology 29 (2016) 475–481.

[17] S. Bibian, G. Dumont, M. Huzmezan, C. Ries, Patient variability and uncertainty quantification in anesthesia: Part I - PKPD modeling and identification, IFAC proceedings 39 (2006) 549–554.

[18] G. A. Dumont, Closed-loop control of anesthesia - A review, IFAC Proceedings Volumes (IFAC-PapersOnline) 45 (2012) 373–378.

[19] K. Soltesz, On automation in anesthesia, Department of Automatic Control, Lund University, Sweden, 2013.

[20] A. Pawlowski, L. Merigo, J. Guzmán, S. Dormido, A. Visioli, Two-degree-of-freedom control scheme for depth of hypnosis in anesthesia, IFAC-PapersOnLine 51 (2018) 72–77.

[21] K. J. Åström, R. Murray, Feedback systems, Princeton university press, 2008.

[22] O. Garpinger, Design of robust PID controllers with constrained control signal activity, Department of Automatic Control, Lund University, 2009.

[23] M. T. Dzindolet, S. A. Peterson, R. A. Pomranky, L. G. Pierce, H. P. Beck, The role of trust in automation reliance, International journal of human-computer studies 58 (2003) 697–718.

[24] W. Goffe, G. Ferrier, J. Rogers, Global optimization of statistical functions with simulated annealing, Journal of Econometrics 60 (1994) 65–99.

[25] K. Svanberg, A class of globally convergent optimization methods based on conservative convex separable approximations, SIAM Journal on Optimization 12 (2003) 555–573.

[26] F. Bagge Carlson, M. Fält, ControlSystems.jl: A control systems toolbox for Julia, 2016.

[27] J. Revels, M. Lubin, T. Papamarkou, Forward-mode automatic differentiation in Julia, 2016.

[28] F. Bagge Carlson, Optimization of controller parameters in Julia using ControlSystems.jl and automatic differentiation, Technical Report, Department of Automatic Control, Lund University), 2019.

[29] J. D. Morse, J. Hannam, B. J. Anderson, Pharmacokinetic–pharmacodynamic population modelling in paediatric anaesthesia and its clinical translation, Current Opinion in Anaesthesiology 32 (2019) 353–362.

[30] K. van Heusden, J. Ansermino, G. Dumont, Performance of robust PID and Q-design controllers for propofol anesthesia, IFAC-PapersOnLine 51 (2018) 78–83.

[31] K. Soltesz, C. Grimholt, S. Skogestad, Simultaneous design of PID controller and measurement filter by optimization, IET Control Theory & Applications 11 (2017) 348–348.